Langmuir
Letter
pubs.acs.org/Langmuir

Rigiflex Lithography-Based Nanodot Arrays for Localized Surface Plasmon Resonance Biosensors

Dong Kyu Park,[†] Hye In Kim,[†] Jun Pyo Kim,[†] Je Seob Park,[‡] Su Yeon Lee,[§] Seung-Man Yang,[§] Jeewon Lee,[∥] Chan-Hwa Chung,[†] Sang Jun Sim,[†] and Pil J. Yoo*[,†,‡]

[†]*School of Chemical Engineering, and* [‡]*SKKU Advanced Institute of Nanotechnology (SAINT), Sungkyunkwan University, Suwon 440-746, Republic of Korea,* [§]*Department of Chemical and Biomolecular Engineering, KAIST, Daejeon 305-701, Republic of Korea, and* [∥]*Department of Chemical and Biological Engineering, Korea University, Seoul 136-701, Republic of Korea*

Received February 9, 2010. Revised Manuscript Received March 25, 2010

We present a facile and robust means of fabricating metallic nanodot arrays for localized surface plasmon resonance (LSPR) biosensors through the strategic coupling of a polymeric template prepared with rigiflex lithography and a subsequent metallization via electrodeposition. Rigiflex lithography provides the capability to realize large-scale nanosized features as well as process flexibility during contact molding. In addition, the electrodeposition process enables wet-based nanoscale metallization with high pattern fidelity and geometric controllability. Generated metallic nanodot arrays can be used as a general platform for LSPR biosensors via the sequential binding of chemicals and biomolecules. Extinction spectra of the corresponding LSPR signal are measured with UV−vis−NIR spectroscopy, from which the pattern size and shape dependence of LSPR are readily confirmed. The feasibility of a very sensitive biosensor is demonstrated by the targeted binding of human immunoglobulin G, yielding subnanomolar detection capability with high selectivity.

Introduction

Noble metal nanoparticles and nanostructures have been extensively exploited in myriad applications on the basis of their unique optical and electronic properties.[1] When metallic nanostructures interact with a light beam, part of the incident photons are absorbed and part are scattered in different directions. During this process, unique optical properties of the localized surface plasmon resonance (LSPR) absorption are obtained over the whole visible and near-infrared (NIR) region. LSPR is an optical phenomenon of nonpropagating plasmon excitations generated by collective oscillations of the conduction band electrons in metal nanostructures surrounded by a dielectric environment when they are excited by incident electromagnetic radiation at a specific wavelength.[2] At the LSPR, the incoming light is absorbed or scattered by the noble metal nanostructures; concurrently, there is a confinement and an enhancement in the electromagnetic field near or on plasmonic nanostructures.[3] The detection of this phenomenon is generally performed by monitoring UV−vis spectral changes in transmission mode. The energy associated with this optical resonance strongly relies on the nanostructure size, shape, interparticle spacing, and dielectric properties of the surrounding medium.[4−7] These properties have enabled a route to sensing in which changes in the peak location and intensity of the characteristic LSPR spectrum offer a very sensitive probe for detecting small changes in the dielectric environment around the nanostructures. This can be utilized to detect and monitor molecular binding events in real time, forming the basis of label-free detection.[8,9] Potential biological applications include immunoassays, protein quantification, cellular imaging, cell sorting, and therapeutic agents.[10]

Toward this goal, most research on LSPR biosensors to date was performed with the intent of establishing surface-immobilized arrays of noble metal nanostructures with targeted LSPR properties.[11−14] A typical approach to forming these nanostructure arrays is to transfer chemically synthesized nanoparticles from suspensions to solid substrates, from which the LSPR properties of an ensemble of nanoparticles can be obtained.[15−17] This scheme is advantageous in that the chemical synthesis allows precise control of the sizes and shapes of the metallic nanoparticles simply by modifying the reaction parameters (i.e., time, temperature, and concentration of the reactants). However, the monodispersity and reproducibility of the desired structures of arrays are rarely achievable using this method. In particular, this technique usually lacks spatial control, causing the problematic agglomeration of nanoparticles.[18] Moreover, deviation in shapes and sizes within

*Corresponding author. E-mail: pjyoo@skku.edu.

(1) Haes, A. J.; Haynes, C. L.; McFarland, A. D.; Schatz, G. C.; Van Duyne, R. R.; Zou, S. L. *MRS Bull.* **2005**, *30*, 368–375.
(2) Willets, K. A.; Van Duyne, R. P. *Annu. Rev. Phys. Chem.* **2007**, *58*, 267–297.
(3) Xia, Y. N.; Halas, N. J. *MRS Bull.* **2005**, *30*, 338–344.
(4) Kelly, K. L.; Coronado, E.; Zhao, L. L.; Schatz, G. C. *J. Phys. Chem. B* **2003**, *107*, 668–677.
(5) Mock, J. J.; Barbic, M.; Smith, D. R.; Schultz, D. A.; Schultz, S. *J. Chem. Phys.* **2002**, *116*, 6755–6759.
(6) Su, K. H.; Wei, Q. H.; Zhang, X.; Mock, J. J.; Smith, D. R.; Schultz, S. *Nano Lett.* **2003**, *3*, 1087–1090.
(7) Mock, J. J.; Smith, D. R.; Schultz, S. *Nano Lett.* **2003**, *3*, 485–491.
(8) Nath, N.; Chilkoti, A. *Anal. Chem.* **2002**, *74*, 504–509.
(9) Anker, J. N.; Hall, W. P.; Lyandres, O.; Shah, N. C.; Zhao, J.; Van Duyne, R. P. *Nat. Mater.* **2008**, *7*, 442–453.
(10) Cao, C.; Sim, S. J. *Biosens. Bioelectron.* **2007**, *22*, 1874–1880.
(11) Endo, T.; Kerman, K.; Nagatani, N.; Takamura, Y.; Tamiya, E. *Anal. Chem.* **2005**, *77*, 6976–6984.
(12) Murphy, C. J.; Gole, A. M.; Hunyadi, S. E.; Stone, J. W.; Sisco, P. N.; Alkilany, A.; Kinard, B. E.; Hankins, P. *Chem. Commun.* **2008**, 544–557.
(13) Yan, B.; Thubagere, A.; Premasiri, W. R.; Ziegler, L. D.; Dal Negro, L.; Reinhard, B. M. *ACS Nano* **2009**, *3*, 1190–1202.
(14) Cao, C.; Sim, S. J. *Lab Chip* **2009**, *9*, 1836–1839.
(15) Frederix, F.; Friedt, J. M.; Choi, K. H.; Laureyn, W.; Campitelli, A.; Mondelaers, D.; Maes, G.; Borghs, G. *Anal. Chem.* **2003**, *75*, 6894–6900.
(16) Dahlin, A.; Zach, M.; Rindzevicius, T.; Kall, M.; Sutherland, D. S.; Hook, F. *J. Am. Chem. Soc.* **2005**, *127*, 5043–5048.
(17) Nusz, G. J.; Marinakos, S. M.; Curry, A. C.; Dahlin, A.; Hook, F.; Wax, A.; Chilkoti, A. *Anal. Chem.* **2008**, *80*, 984–989.
(18) Zhang, S. S.; Leem, G.; Srisombat, L. O.; Lee, T. R. *J. Am. Chem. Soc.* **2008**, *130*, 113–120.

different batches discourages the use of this technique for fabricating nanostructures with reproducible, consistent plasmonic properties.

Recent improvements in nanolithographic fabrication have enabled precise tuning of the LSPR to optimize the optically enhanced properties based on the immobilized metallic nanostructures. Top-down-based patterning approaches such as photolithography, electron-beam lithography, and focused ion-beam lithography have been adopted to obtain arrays of metallic nanostructures on solid substrates via selective etching or deposition processes.[19] These methods are capable of generating arbitrary patterns of metallic nanostructures with accurate control over spatial distribution as well as specific sizes and shapes. However, these techniques are expensive, and the patterned regions are relatively small (i.e., low throughput), which limits their applicability to commercialized sensing devices. Another lithographic means to attaining the structured arrays includes nanosphere lithography in which a template formed by the self-assembly of monodispersed colloidal nanospheres on flat surfaces is exploited as an etching and/or deposition mask.[20−22] Nanosphere lithography provides a low-cost, high-throughput processing means of fabricating highly ordered nanostructure arrays. However, this technique also faces similar limitations as observed in other chemical synthesis or lithographic methods, entailing issues of surface coverage, defects, and the geometric constraints imposed by the nanosphere mask on the periodic particle array. Specifically, only triangular or hexagonally shaped metal nanostructures can be produced from deposition through the stacked layers of close-packed nanospheres.

To address these shortcomings and allow for precisely controlled LSPR properties in immobilized metallic nanostructure arrays, unconventional lithographic techniques are available that readily provide advantages of geometric and spatial controllability of the patterns as well as low-cost and high-throughput processing. The nanoimprint lithographic method, for example, has been extensively investigated for fabricating metal nanostructure arrays for tunable LSPR properties.[23,24] Moreover, recently proposed means of soft imprint lithography has provided the capability to observe LSPR signals directly for surface-binding events with high resolution and sensitivity.[25−27] One of the most important aspects of nanoimprint lithography (NIL) is that the size and shape of the replicated patterns are very dependent on the mechanical properties of the mold material because the conditions for the physical contact of the mold are crucial to the patterning results of the NIL process. When the mold is made of a rigid, hard material, NIL can allow pattern resolution down to 10 nm features. However, when the mold is made of a soft, deformable material as in soft lithography where poly(dimethylsiloxane) is used,[28−30] one can obtain relatively large patterns because the patterned structures of a mold are vulnerable to mechanical deformation during contact with the substrate.[31]

Meanwhile, the rigidity of the mold can be an obstacle to obtaining flexibility in managing the patterning process. Although extremely flat substrates are required for high-pressure processing in NIL, in soft lithography, curved substrates can be patterned through conformal contact with a freely deformable mold. One may conceive of a means of patterning that can be derived from simultaneously combining the advantages of the mechanical rigidity of the mold pattern in NIL and the deformable flexibility in soft lithography. Although it may sound counterintuitive, rigiflex lithography can produce this scheme through attaching rigid structures of nanoscale patterns onto the flexible supporting substrate.[32] In rigiflex lithography, modulus-enhanced poly(urethane acrylate) (PUA) is molded and UV-cured onto a flexible support of poly(ethylene terephthalate) (PET), from which not only high flexibility and high fidelity processing but also a pattern resolution down to the sub-100-nm scale can be obtained concurrently.[33−35]

In the present study, we fabricate nanoscale hole-patterned arrays of polymer (diameter 150−550 nm) over a large-scale area using rigiflex lithography and then further utilize it as a template to generate gold nanodot arrays by electrodeposition. To apply the prepared metal array to sensing devices, we investigate the LSPR at the surface of Au nanodot arrays with the sequential binding of biomolecules. As a result, we can conclude that the peak shift of the extinction spectra of LSPR is strongly dependent on the functionalized condition of the Au surface as well as the pattern size and height of the nanodot array. Along with obtaining tunable LSPR properties, the sensitivity and selectivity of metallic nanodot arrays as label-free biosensors are also investigated through the targeted binding of human immunoglobulin G. Thereby, we demonstrate the capability for subnanomolar detection along with the prevention of the nonspecific binding of other biomolecules onto the nanodot arrays.

Experimental Section

Fabrication of a UV-Curable Mold. The PUA mold consists of a functionalized prepolymer (MINS 311RM, Minuta Tech., Korea) with urethane acrylate groups, a photoinitiator, and a radiation-curable releasing agent for surface activity.[33,34] The photoinitiator used in this study was 1-hydroxycyclohexylphenylketone (Irgacure 184, Ciba Specialty Chemicals, Switzerland). Commercial acrylate-organomodified polysiloxane (Rad 2200N, TEGO Chemie Service, Germany) was used as a releasing agent and provided compatibility with the UV-curing process. The liquid composite material was drop dispensed onto a master pattern. A flexible, transparent support made of PET was brought into contact with the coated composite liquid. Subsequently, it was exposed to UV light (λ = 250−400 nm) for 30 s through the transparent back side (dose = 100 mJ/cm^2). After UV curing, the mold was easily peeled off of the master. Trimming the edges completed the preparation of the replicated PUA mold.

Pattern Formation by Rigiflex Lithography. The experimental procedure used for patterning is schematically depicted in Figure 1. For pattern formation by rigiflex lithography, cleaned substrates of a glass cover slide or a flexible PET film were first

(19) Grand, J.; Adam, P. M.; Grimault, A. S.; Vial, A.; De la Chapelle, M. L.; Bijeon, J. L.; Kostcheev, S.; Royer, P. *Plasmonics* **2006**, *1*, 135–140.
(20) Hulteen, J. C.; Treichel, D. A.; Smith, M. T.; Duval, M. L.; Jensen, T. R.; Van Duyne, R. P. *J. Phys. Chem. B* **1999**, *103*, 3854–3863.
(21) Haes, A. J.; Van Duyne, R. P. *J. Am. Chem. Soc.* **2002**, *124*, 10596–10604.
(22) Haes, A. J.; Hall, W. P.; Chang, L.; Klein, W. L.; Van Duyne, R. P. *Nano Lett.* **2004**, *4*, 1029–1034.
(23) Kim, S.; Jung, J. M.; Choi, D. G.; Jung, H. T.; Yang, S. M. *Langmuir* **2006**, *22*, 7109–7112.
(24) Lucas, B. D.; Kim, J. S.; Chin, C.; Guo, L. *J. Adv. Mater.* **2008**, *20*, 1129–1134.
(25) Stewart, M. E.; Mack, N. H.; Malyarchuk, V.; Soares, J. A. N. T.; Lee, T. W.; Gray, S. K.; Nuzzo, R. G.; Rogers, J. A. *Proc. Natl. Acad. Sci. U.S.A.* **2006**, *103*, 17143–17148.
(26) Yao, J. M.; Stewart, M. E.; Maria, J.; Lee, T. W.; Gray, S. K.; Rogers, J. A.; Nuzzo, R. G. *Angew. Chem., Int. Ed.* **2008**, *47*, 5013–5017.
(27) Stewart, M. E.; Yao, J. M.; Maria, J.; Gray, S. K.; Rogers, J. A.; Nuzzo, R. G. *Anal. Chem.* **2009**, *81*, 5980–5989.
(28) Xia, Y. N.; Whitesides, G. M. *Annu. Rev. Mater. Sci.* **1998**, *28*, 153–184.
(29) Henzie, J.; Lee, M. H.; Odom, T. W. *Nat. Nanotechnol.* **2007**, *2*, 549–554.
(30) Suh, K. Y.; Kim, Y. S.; Lee, H. H. *Adv. Mater.* **2001**, *13*, 1386–1389.
(31) Delamarche, E.; Schmid, H.; Michel, B.; Biebuyck, H. *Adv. Mater.* **1997**, *9*, 741–746.
(32) Suh, D.; Choi, S. J.; Lee, H. H. *Adv. Mater.* **2005**, *17*, 1554–1560.
(33) Choi, J. H.; Kim, D.; Yoo, P. J.; Lee, H. H. *Adv. Mater.* **2005**, *17*, 166–171.
(34) Yoo, P. J.; Choi, S. J.; Kim, J. H.; Suh, D.; Baek, S. J.; Kim, T. W.; Lee, H. H. *Chem. Mater.* **2004**, *16*, 5000–5005.
(35) Kim, P.; Suh, K. Y. *Langmuir* **2007**, *23*, 4549–4553.

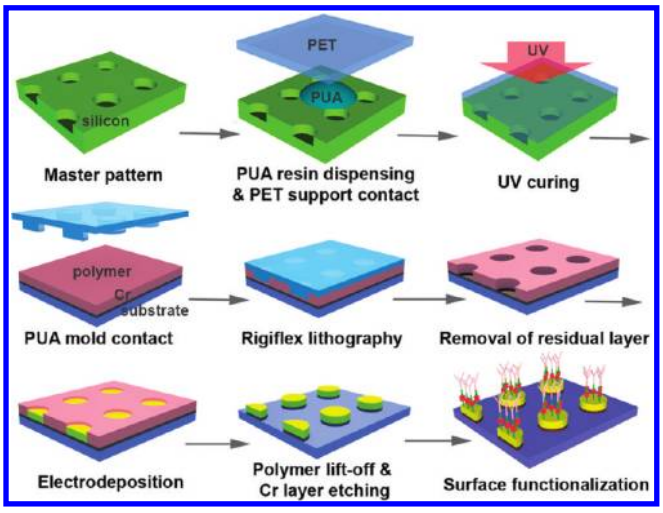

Figure 1. Schematic illustration of the patterning and surface functionalization of nanodot arrays. Rigiflex lithography is employed to make negatively replicated nanohole array of polymer, followed by electrodeposition over a polymeric template for the selective growth of gold to generate positively patterned nanodot arrays.

vacuum deposited with chromium to a 10 nm thickness to serve as a conducting electrode for electrodeposition as well as an adhesion-promoting layer for gold. Then, the substrates were spin coated with polystyrene (PS, M_n = 404 200 g/mol, M_w/M_n = 1.05, Polymer Source Inc., Canada) or poly(methyl methacrylate) (PMMA, M_n = 546 000 g/mol, M_w/M_n = 1.11, Polymer Source Inc.) in toluene to the desired thicknesses. The samples were in turn baked in a vacuum oven at 70 °C for 1 h to remove any residual solvent in the polymer film. A PUA mold was then placed on the polymer, and a 5-mm-thick poly(dimethylsiloxane) block was placed onto the mold as a buffer layer for the uniform distribution of pressure. Then, the temperature of the samples was elevated (105 °C for PS and 125 °C for PMMA) above the T_g of the polymer while applying a slight pressure of 0.5−1.0 MPa for 30 min. To avoid any unexpected deformation in the polymeric layer due to the difference in thermal expansion coefficients between the PUA mold and the polymer, PUA molds were carefully placed on the polymer after preheating the sample to 80 °C and were removed after cooling the sample to 80 °C. A thin residual layer of the polymer remaining in places where the PUA mold was in contact was removed by a short plasma treatment (air plasma, 30 s to 1 min) using a conventional plasma cleaner (PDC-001, Harrick Scientific Corp.).

Fabrication of Au Nanodot Array. Two metallization approaches have been adopted for the templated growth of Au nanodot arrays: sputtering and electrodeposition. Gold sputtering was carried out in an ion coater (HC-21, Hoyeon Tech., Korea) to a thickness of 30 nm. The dc electrodeposition of gold was conducted with an electrochemical workstation (WPG 100e, Won-A Tech, Korea). A three-electrode electrochemical cell with a chronoamperometry cycle was employed, which consists of a saturated calomel reference electrode (SCE), a platinum mesh counter electrode, and a chromium-layer working electrode. Au nanodots were grown inside the polymeric patterns directly onto the conductive Cr layer from an aqueous solution of 40 g/L $KAu(CN)_2$ and 100 g/L KH_2PO_4. The cell voltages were kept at −1.8 V vs the SCE electrode for 10 s, yielding 120−150-nm-thick Au nanodots. Lift-off for the polymeric patterns was performed by immersing the samples in toluene (for PS) or acetone (for PMMA) and using a low-power ultrasonic bath. The remaining Cr layer was removed with etching in a standard etchant (Cr-75k, CYANTEK Co.). After the completion of the lift-off process, samples were rinsed with methanol and water and dried with nitrogen. Generated Au nanodot patterns were examined by scanning electron microscopy (FE-SEM, JSM7401F, JEOL, Japan) or atomic force microscopy (AFM, Innova, Veeco, Plainview, NY) in tapping mode.

Test for LSPR Biosensors. To immobilize anti-IgG antibodies onto the Au nanodot array, the following chemical-modification process was employed. First, 16-mercaptohexadecanoic acid (2 mM in ethanol, Aldrich) was used to generate COOH groups on the patterned Au surface. The COOH-terminated surface can easily be converted into a protein-bound surface using a two-step coupling reaction. First, the terminal COOH groups were activated by reacting with *N*-hydroxysulfosuccinimide (Sulfo-NHS, 2 mM, Pierce) and 1-ethyl-3-(3-dimethylaminopropyl) carbodiimide (EDC, 5 mM, Pierce) for 30 min, generating amine-reactive NHS esters on the surface. To couple biotin covalently to the surface, an amine-containing biotin, biotinyl-3,6-dioxaoctanediamine (EZ-Link biotin-PEO-amine, 50 mM, Pierce) in a (2-*N*-morpholino)ethanesulfonic acid buffer (MES, pH 4.7−5.5, 0.1 M, Pierce) was applied for 30 min. Streptavidin (Pierce) was diluted to 10 μg/mL in PBS, reacted with the biotins for 30 min, washed with PBS, and dried with nitrogen. Then, the monoclonal antihuman IgG-Biotin antibody (Sigma-Aldrich) was diluted to 10 μg/mL in PBS, reacted with streptavidin for 1 h, washed with PBS, and dried with nitrogen. The extinction measurements were recorded with a UV−vis−NIR spectrometer (UV-3600, Shimadzu, Japan) over the range of 350−2500 nm.

Results and Discussion

To fabricate a template for Au nanodot arrays, the polymeric layer on the Cr-coated glass or PET substrate was first put in contact with the rigiflex mold of PUA and molded under elevated-temperature conditions (> T_g), yielding variously sized nanohole array patterns. In the course of the molding process, slight pressure was applied to the PUA mold to promote the rate of capillarity of the softened polymeric layer within the confined structures of the PUA mold, ultimately leading to the generation of negatively replicated structures of the polymer on the surface.[30,32] The left column in Figure 2 shows the results of replicated polymeric patterns, wherein the diameter ranges from 150 to 350 and 550 nm. No noticeable defects are observed over a large area (8 × 12 mm^2); therefore, the polymeric structures offer an ideal template for the further process of metallization. Careful control of the initial film thickness of the polymer to account for the surface-to-volume ratio of the PUA mold pattern can ideally lead to the formation of a completely filled mold without leaving any residual polymer in the interstitial regions between the molded features. In this case, however, the intrinsic surface roughness of the Cr-deposited glass or PET substrate hinders the complete dewetting and subsequent opening of the polymeric layer; therefore, a very thin residual layer of polymer is retained between the PUA mold and the substrate.[36] Therefore, plasma cleaning was employed for 30−60 s to eliminate this thin residual layer, exposing the original substrate underneath. Then, electrodeposition was performed for selective Au growth only in places where the electroconducting Cr layer is exposed, resulting in the formation of Au nanodots, the height of which is close to that of the polymeric template (120−150 nm). The right column in Figure 2 shows the results of Au nanodot arrays fabricated using this method. Although some irregularities in shape and size are observed for smaller dot arrays, it is clear that very dense metallic nanodot arrays can readily be fabricated through this cost-effective nonphotolithographic means of patterning.

In a general preparation of the patterned polymeric template, a representative thermoplastic polymer such as PS or PMMA is

(36) Lenz, P. *Adv. Mater.* **1999**, *11*, 1531–1534.

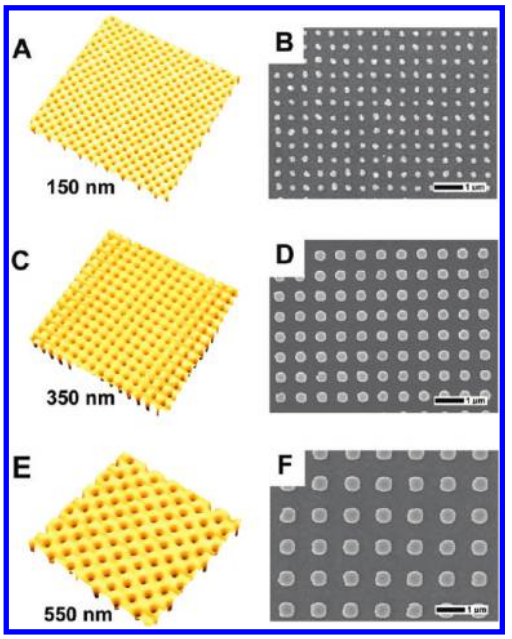

Figure 2. Atomic force microscopy images (left column) for the polymeric nanohole template and scanning electron micrographs (right column) of the electrodeposited Au nanodot array. The scan size of the AFM images is 10 μm × 10 μm. Diameter of Au nanodots: (A, B) 150 nm, (C, D) 350 nm, and (E, F) 550 nm.

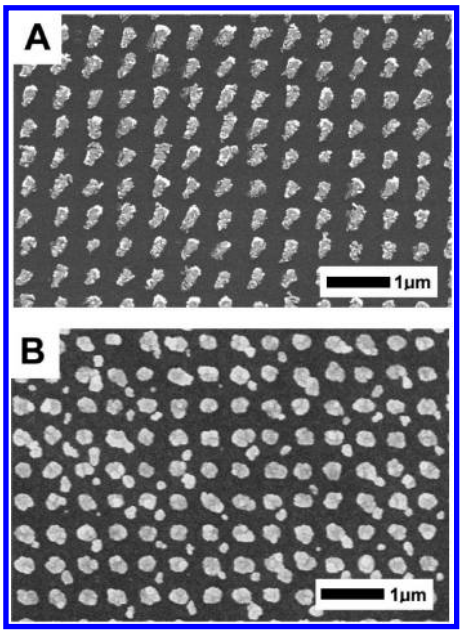

Figure 3. Scanning electron micrographs for examples of pattern failure. (A) Use of low-molecular-weight polymer (MW of PS ≈ 13 000) leads to the failure to control the polymeric capillarity during rigiflex lithography. Nonuniform capillarity and resulting pattern distortion occur because of the increased mobility and fluctuational instability of the polymer. (B) Use of water-permeable PMMA results in pattern failure during electrodeposition. Moisture uptake of PMMA under aqueous condition of electrodeposition brings about the unexpected growth of Au in the interstitial areas between patterns.

used as a molding material because of its availability and well-established physical properties. With regard to material selection of the polymer for stringent pattern fidelity, the results presented in Figure 3 explain the influences of molecular weight and type of polymer on the successful realization of patterning. In our experiment, we use a relatively high molecular weight polymer (MW ≈ 400 000) to maintain good controllability over the fluidic behavior of the polymeric film at high temperature above T_g.[37] Under such a condition, the undulational instability can be minimized and wetting-induced capillarity can accordingly be maximized because of the highly entangled structure of the polymeric chains.[38,39] However, when a polymer molecular weight that is smaller than the entanglement molecular weight is used (PS, MW ≈ 13 000), the fluidic behavior of the polymeric film is pronounced and the thin film instability plays an important role in the deformation of the polymeric layer. The initial mold contact localizes the directional movement of the polymeric layer, which subsequently drives film thinning and accelerates dewetting, giving rise to the formation of irregularly formed nanoholes, as shown in Figure 3A.[40]

Figure 3B shows the result of final Au nanodot arrays after templated electrodeposition onto the PMMA patterns, wherein a randomly disordered, interstitially grown Au nanodot array is observed. In general, PMMA provides better mechanical properties (tensile strength: 55−80 MPa) and a smaller coefficient of thermal expansion (CTE ≈ 6.9×10^{-5}/K) than those of PS (~46−60 MPa, ~8×10^{-5}/K).[41] These properties can mitigate unwanted deformations of the polymer during molding, thereby making PMMA more suitable for nanoscale polymeric molding. However, PMMA has the intrinsic drawback of partial permeability to water (moisture uptake up to 1 to 2 wt %),[41] which is troublesome in the aqueous environment of the electrodeposition process. When PMMA is used as a template for electrodeposition, therefore, the penetration of water through a thin layer of PMMA and the resulting formation of electroconduction channels therein allows random Au electrodeposition at the interface between PMMA and the Cr-coated substrate. Therefore, for a successful combination of polymeric nanomolding and templated electrodeposition, PS rather than PMMA should be chosen because PS has superior resistance to water permeation.

It has been reported that the height of metallic nanostructures can strongly affect their LSPR characteristics.[24,42,43] Two metallization approaches used in this study—electrodeposition via a wet process and sputtering via a vacuum process—can be used to fabricate arrays of different heights. Alternatively, other types of vacuum deposition techniques such as thermal evaporation or electron beam evaporation can be employed as well. These methods are advantageous over sputtering in that the undesirable interfacial damage and sidewall deposition can be minimized. However, evaporation-based deposition is accompanied by the problem of radiant heating for the substrate usually above the glass-transition temperature of the polymers (PS or PMMA), which can lead to a deformation or collapse of the patterned polymeric structures. Therefore, sputtering was chosen as a representative method for the vacuum deposition of Au in this study. In general, sputtering the metal can generate a uniformly deposited film onto the entire surface irrespective of the surface topography, thus there is no selectivity in the film deposition

(37) Masson, J. L.; Olufokunbi, O.; Green, P. F. *Macromolecules* **2002**, *35*, 6992–6996.
(38) Suh, K. Y.; Seo, S. M.; Yoo, P. J.; Lee, H. H. *J. Chem. Phys.* **2006**, *124*, 024710.
(39) Suh, K. Y.; Lee, H. H. *J. Chem. Phys.* **2002**, *117*, 6266–6270.
(40) Sharma, A.; Reiter, G. *J. Colloid Interface Sci.* **1996**, *178*, 383–399.
(41) Mark, J. E. *Polymer Data Handbook*; Oxford University Press: New York, 1999.
(42) Jensen, T. R.; Malinsky, M. D.; Haynes, C. L.; Van Duyne, R. P. *J. Phys. Chem. B* **2000**, *104*, 10549–10556.
(43) Kim, S.; Cheng, N.; Jeong, J. R.; Jang, S. G.; Yang, S. M.; Huck, W. T. S. *Chem. Commun.* **2008**, 3666–3668.

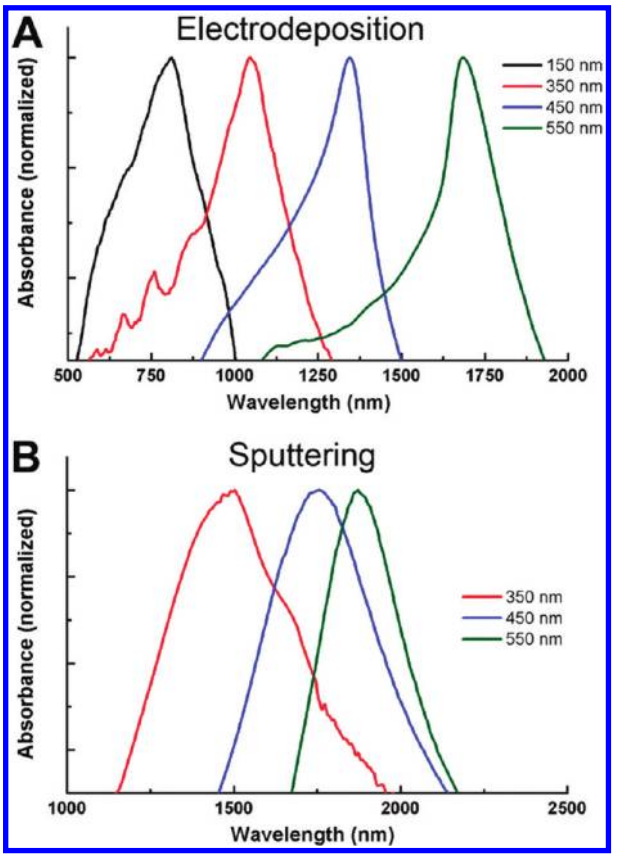

Figure 4. Effect of pattern size and height of Au nanodot arrays on the LSPR peak wavelength characterized with UV−vis−NIR absorption spectra. (A) Tuning of the LSPR peak wavelength by varying the diameter of electrodeposited nanodots (pattern height ∼150 nm). (B) Tuning of the LSPR peak wavelength by varying the diameter of sputtered nanodots (pattern height ∼30 nm).

depending on whether the surface is a polymeric template or a surface-exposed substrate. As a result, during lift-off, a fully interconnected film of sputtered Au can be peeled off along with the polymeric layer and may fail to maintain the pattern selectivity. This characteristic eventually restricts the thickness of sputtered Au layers up to several tens of nanometers and confines the attainable minimum feature size down to several hundreds of nanometers. Electrodeposition has no restrictions on tailoring the shape or the size of the metal patterns as long as the structure of the polymeric template can clearly be defined, wherein gold growth selectively occurs atop the surface-exposed regions of the pattern.[44]

LSPR properties of the fabricated Au nanodot arrays were investigated by recording the extinction spectra (absorption + scattering). Figure 4A,B show the results of UV−vis−NIR absorption spectra of Au nanodot array prepared by electropdeposition (Figure 4A, thickness of Au = 150 nm) and sputtering processes (Figure 4B, thickness of Au = 30 nm), respectively. Because of the aforementioned issue related to pattern resolution for a sputtered film, Au nanodots with 150 nm diameter can be obtained only from the electrodeposition process. Changing the diameter of the electrodeposited nanodots with 150 nm height (i.e., to an oblate spheroid with a relatively small diameter to height ratio) allows for tuning of the LSPR peak wavelength ranging from approximately 800 to 1700 nm. However, decreasing the height of the nanodots (∼30 nm, disk with a relatively large

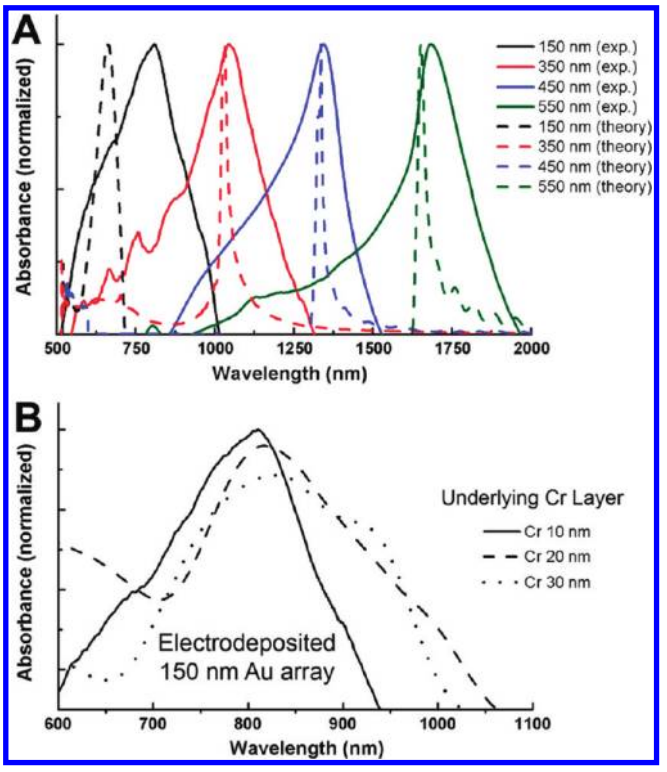

Figure 5. (A) Comparison between FDTD calculated (---) and experimental (−) absorption spectra of an electrodeposited Au nanodot array with different diameters (pattern height ∼150 nm). (B) Effect of thickness of the underlying Cr layer on the LSPR response.

diameter to height ratio) by sputtering instead of electrodeposition causes the LSPR to shift to much longer wavelengths (1500−1900 nm). In both cases, the maximum in surface plasmon absorption spectra is red shifted in response to the increase in pattern size, a trend consistent with Mie theory.[2,45] Furthermore, decreasing the thickness of the Au nanodots causes the LSPR to shift to longer wavelengths. This indicates a strong dependence of the LSPR on the nanostructure shape, leading to red shifting as the pattern becomes more oblate.[4,46]

To elucidate the character of the LSPR modes and to explore the source of absorbance, finite-difference time-domain (FDTD) calculations were performed using geometric parameters that are identical to fabricated Au nanodot structures by electrodeposition (Au thickness of 150 nm). In this modeling, the parameter conditions of the spatial mesh size ($\Delta x = \Delta y = \Delta z = 3.33$ nm) and time step ($\Delta t = 5.56 \times 10^{-18}$ s) are chosen to ensure the Courant stability condition. Linearly polarized plane waves are illuminated on the Au oblate spheroid arrays at normal incidence. The auxiliary differential equation method based on the single-pole Drude model is adopted to simulate the plasmonic behavior of Au nanostructures. To calculate the absorbance of gold nanostructures, the periodic boundary conditions are applied in two horizontal directions (x and y). Results of FDTD modeling are presented and compared with experiments in Figure 5A. For Au nanodot arrays with diameters of 350, 450, and 550 nm, experimental results are in good agreement with calculated peak positions. For 150 nm Au nanodot arrays, however, there is a deviation between experiments and modeling, which may arise from a slight widening of the diameter of the Au nanaodot pattern

(44) Wang, Y.; Deng, J. J.; Di, J. W.; Tu, Y. F. *Electrochem. Commun.* **2009**, *11*, 1034–1037.

(45) Mie, G. *Ann. Phys.* **1908**, *25*, 377–445.

(46) Larsson, E. M.; Alegret, J.; Kall, M.; Sutherland, D. S. *Nano Lett.* **2007**, *7*, 1256–1263.

during electrodeposition. Notably, the calculated peak widths are smaller than the measured ones, indicative of imperfect surface conditions for electrodeposited Au patterns such as defects and inhomogeneity in size and morphology. Surface roughening of Au nanodots due to the intrinsic nature of the electrodeposition process can be ascribed to contribute to this structural inhomogeniety, though it does not appear to affect the optical properties and the resulting peak position.[46] Overall, we observed qualitative good agreement between the experimental observations and the FDTD calculation results.

As previously reported,[47,48] the presence of a Cr layer underneath the Au nanodots weakens the LSPR peak intensity and broadens the LSPR bandwidth. In this study, a 10 nm thickness of the Cr layer was used as the support for electrodeposited Au nanodot arrays, which was the minimum thickness determined from experiments to obtain enough electroconductivity for the electrodeposition. As shown in Figure 5A, there is slight peak broadening as the pattern size decreases. The observed broadening of the LSPR spectra for smaller patterns can primarily be ascribed to the presence of the thin Cr adhesion layer, which has not been considered in the above FDTD modeling. This result indicates that the LSPR properties of Au nanodot arrays are compromised by the existence of the Cr interfacial layer, a component essentially required for the electroconductivity for electrodeposition as well as the structural stability of Au on the substrate. To investigate the influence of Cr layer thickness on LSPR signals, we prepared samples of 150 nm Au nanodot arrays with increased underlying Cr layer thickness to 20 and 30 nm and tested them for LSPR. As shown in Figure 5B, though a very slight red shift is observed, varying the thickness of the Cr layer rarely affect the LSPR peak wavelength. However, it causes the generation of peripheral peaks around the centroid and reduces the intensity of the LSPR, thus the use of the minimum thickness of the Cr layer (10 nm) is required.

In a proof-of-principle experiment, nanodot arrays fabricated by rigiflex lithography were used in a real-time, label-free biosensing system. Sequential binding of small biomolecules onto Au nanodots was tested, and the corresponding changes in LSPR were monitored to confirm the protein adsorption and molecular recognition events. Human immunoglobulin G (IgG) proteins and their functions have been well investigated and recognized.[49] As compared to other immunoglobulins in the blood and lymph fluids, IgG antibodies play a dominant role in antigen recognition, providing the majority of antibody-based immunity against hostile viruses or bacteria.

Figure 6 shows the UV−vis−NIR absorption spectra taken after each step of binding onto the Au nanodot arrays from biotin and streptavidin to the IgG antibody, whereby the influence of molecular binding and the corresponding changes in refractive index on the LSPR signal could be investigated. The LSPR spectral shift ($\Delta\lambda$) in accordance with the changes in refractive index can be described as[9,49]

$$\Delta\lambda = m(n_a - n_m)[1 - \exp(-2d/l_d)] \quad (1)$$

where m is the sensitivity factor, n_a and n_m are the refractive indices of the adsorbate layer and the bulk medium, respectively, d is the layer thickness on the metal surface, and l_d is the electromagnetic field decay length. According to eq 1, the addition of each new layer results in a red shift of the LSPR peak maximum,[50] which can be expected from a gradual increase in the effective refractive index with increasing layers of binding around Au nanodots. As seen from Figure 6, sequential binding of biotin, streptavidin, and antihuman IgG-biotin antibody on the Au nanodot arrays leads to a red shift of the LSPR peak maximum for both 150 and 550 nm arrays. It has been observed that a gradual red shift in the LSPR peak maximum proceeded in accordance with a thickening of the coated polymeric layer around the surface of Au nanopatterns, wherein the thickness change in the dielectric environment could quantitatively be monitored.[51] Notably, in this study, because the molecular weight

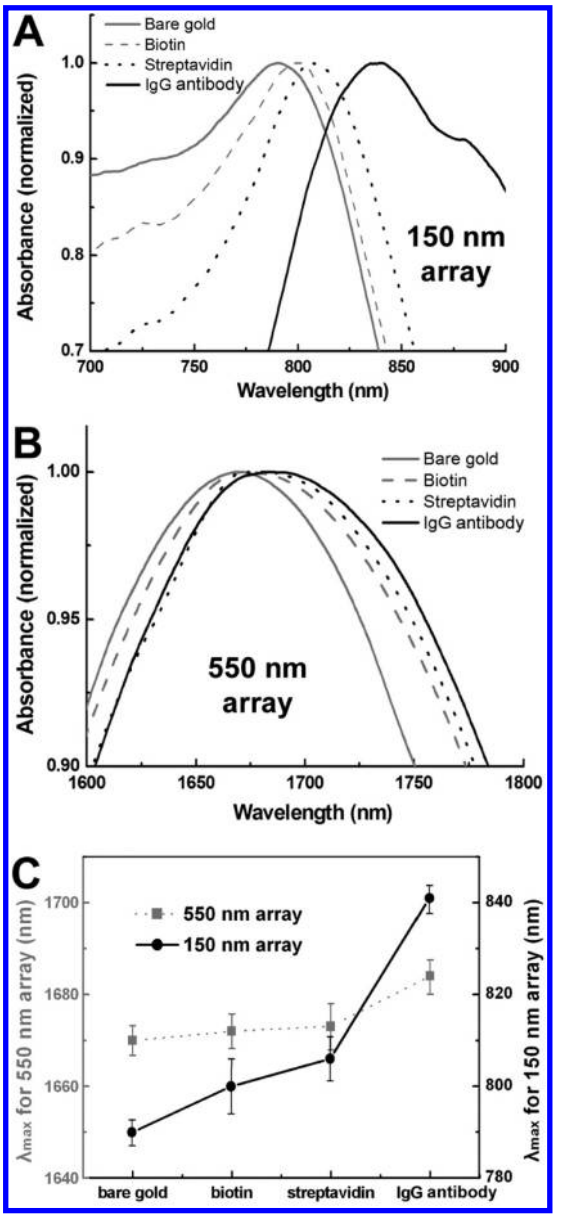

Figure 6. Evolution of the LSPR peak maximum with sequential functionalization of Au nanodot arrays. Diameter of Au nanodots: (A) 150 and (B) 550 nm. (C) Comparison of the red shift of the LSPR peak maximum between the 150 nm array (black circles and solid line) and the 550 nm array (gray squares and dotted line). Error bars show standard deviations.

(47) Zheng, Y. B.; Jensen, L.; Yan, W.; Walker, T. R.; Juluri, B. K.; Jensen, L.; Huang, T. J. *J. Phys. Chem. C* **2009**, *113*, 7019–7024.
(48) Zheng, Y. B.; Juluri, B. K.; Mao, X. L.; Walker, T. R.; Huang, T. J. *J. Appl. Phys.* **2008**, *103*, 014308.
(49) Bendikov, T. A.; Rabinkov, A.; Karakouz, T.; Vaskevich, A.; Rubinstein, I. *Anal. Chem.* **2008**, *80*, 7487–7498.
(50) Hanarp, P.; Kall, M.; Sutherland, D. S. *J. Phys. Chem. B* **2003**, *107*, 5768–5772.
(51) Marinakos, S. M.; Chen, S. H.; Chilkoti, A. *Anal. Chem.* **2007**, *79*, 5278–5283.

of the IgG-biotin antibody (MW ≈ 150 000) is larger than those of biotin (MW ≈ 230) and streptavidin (MW ≈ 50 000), the binding of biotinilated IgG to streptavidin causes a significant thickening of the dielectric around Au, thereby inducing a pronounced peak shift in the LSPR.

The ability to fine tune the LSPR properties by varying the size of the nanopatterns is a key factor in advancing and optimizing LSPR-based sensors. As previously reported, under the condition of immersion in liquid media with different refractive indices, LSPR sensitivity increases in response to an increase in the size of the nanopatterns.[17,46] However, when the specific binding event is of interest inside the aqueous environment, an infinitesimal change in the refractive index around the Au nanopatterns becomes significant and the smaller patterns can meet the need for enhanced LSPR sensitivity. In our study, size effects of the Au nanopatterns are contrasted for 150 and 550 nm arrays as shown in Figure 6C. While about a 50 nm red shift (from 790 to 840 nm) in the LSPR peak maximum is observed for the 150 nm nanodot array, only a 12 nm shift (from 1670 to 1682 nm) can be obtained from a 550 nm nanodot array. In general, as the size of the nanostructure gets smaller, more energy is required to excite the Au and a shorter LSPR peak maximum position is detected accordingly. However, because of the decrease in the total volume capacity for the smaller Au patterns, the intensity of LSPR from bare Au is weakened in response to an increase in size. Therefore, the binding event of a specific molecule with an infinitesimal volume can be detected with an amplified LSPR signal, particularly onto the smaller Au nanopattern array, which can offer increased sensing ability in biosensors. In our experiments, therefore, a 150 nm nanodot array was chosen as a feasible platform for biosensors because of its advantages of an enhanced peak shift in LSPR and robust, large-area applicability.

To assess the biosensing capability in our LSPR biosensors, proteins of human IgG (hIgG) of various concentrations were reacted with the surface-immobilized IgG antibody and the corresponding changes in the peak shift of LSPR were monitored. As a result, a red shift of 7 nm in the LSPR peak maximum was obtained from 1 μg/mL (6.7 nM) hIgG. These changes in the peak shift were weakened with decreasing hIgG concentration: 4 nm shift for 0.1 μg/mL and 3 nm shift for 0.01 μg/mL (Figure 7A). If a smaller Au patterned array is used, then enhanced sensing ability can be expected. Additionally, to check the selectivity of Au nanopattern arrays and to alleviate the concern of nonspecific binding onto the array, other types of proteins (fibrinogen and bovine serum albumin (BSA)) were applied to the IgG-antibody-immobilized array. The resulting LSPR was compared with the control samples. As shown in Figure 7B, no noticeable peak shift was observed (less than 1 nm); therefore, the peak shift of LSPR is mainly driven by the specific binding of biomolecules onto the Au nanodot array. These results also confirm that the presence of some nonspecifically bound proteins onto the surface will not significantly affect the sensitivity of these LSPR biosensors unless they cover the majority of a sample surface. However, when the extent of surface coverage with these proteins is seriously intensified, a problematic case of surface fouling can possibly be encountered.

Finally, to demonstrate the feasibility of large-scale sensor production and the applicability to roll-to-roll processing of flexible biosensors, we prepared a sample of Au nanodot arrays on a flexible PET substrate as shown in Figure 8. Au nanodots (150 nm) were densely patterned over a 8 × 12 mm^2 area with few defects. Though 150 nm nanodot arrays separated by 350 nm were achieved as the smallest feature in this study, it is expected

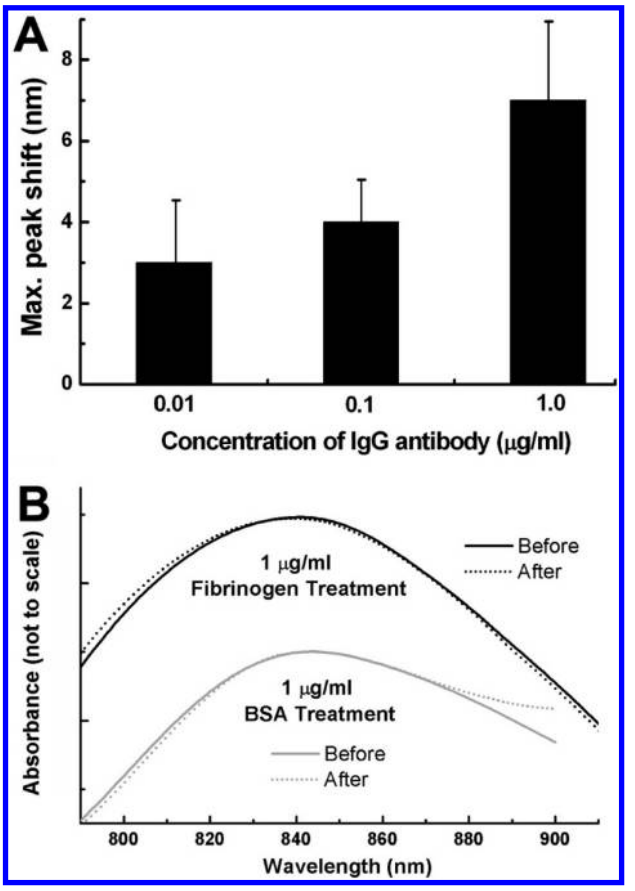

Figure 7. (A) Detection of human IgG by varying the concentration ranging from 0.01 to 1.0 μg/mL. Error bars show standard deviations. (B) LSPR responses of the 150 nm Au nanodot array to the binding of other types of proteins of fibrinogen (black) and bovine serum albumin (gray).

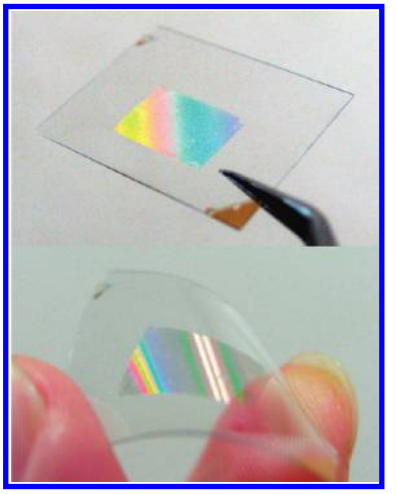

Figure 8. Demonstration of nanodot array fabrication (diameter ~150 nm) onto the flexible PET substrate.

that much smaller patterns can readily be fabricated as long as the master for rigiflex lithography with the required dimension can be prepared. A study on decreasing the pattern size through applying conditional wet etching of Au nanodot patterns is under investigation. Therefore, the entire scheme of patterning suggested in this study, consisting of rigiflex lithography on a flexible substrate followed by metallization with electrodeposition, can be useful in the mass production of nanoarrays, in which neither an expensive

photolithographic patterning process nor a sophisticated vacuum process is needed.

Conclusions

We have demonstrated a method of fabricating metallic nanodot arrays over large-scale areas on the basis of rigiflex lithography and electrodeposition. In rigiflex lithography, precisely controlled experimental conditions were employed to control the capillarity of the thermally softened polymeric film, leading to the formation of polymeric templates of nanohole arrays. Subsequently, electrodeposition was performed to deposit gold selectively onto surface-exposed areas, eventually yielding Au nanodot arrays. To utilize these arrays for LSPR sensing applications, they were treated with sequential binding of biomolecules. As a result, the peak shift in the extinction spectra of LSPR was monitored with UV−vis−NIR spectroscopy, and a strong dependence of the LSPR peak shift on the pattern size and nanodot height was confirmed. As compared to conventional nanoparticle-based LSPR biosensors where concerns related to reproducibility or spatial controllability are encountered, this method offers several advantages for providing a general platform of commercialized LSPR biosensors in practice, which includes the aspects of cost-effective parallel processing, flexible substrates for portable biosensors, small sample volumes, and optimized sensing capabilities for small biomolecules.

Acknowledgment. This work was mainly supported by the National Research Foundation of Korea (KRF) through a grant funded by the Korea Government (MEST) (2009-0085681) and a National Platform Technology grant (10033871) from the Ministry of the Knowledge Economy of Korea. This work was also supported by a New & Renewable R&D program (2009-T1000100282) under the Ministry of the Knowledge Economy of Korea. S.J.S. acknowledges support from the NRL program (no. R0A-R0A-2008-000-20078-0).